REPORT DOCUMENTATION PAGE

Form Approved
OMB No. 0704-0188

1. REPORT DATE *(DD-MM-YYYY)*	2. REPORT TYPE	3. DATES COVERED *(From - To)*
16-07-2012	Conference Paper	

4. TITLE AND SUBTITLE

Thermal Modeling and Performance Measurements of Radiometric Arrays for Near Space Propulsion

5a. CONTRACT NUMBER

5b. GRANT NUMBER

5c. PROGRAM ELEMENT NUMBER

6. AUTHOR(S)
Bosworth, R.; Ventura, A.; Webb, R.; Ketsdever, A.; Gimelshein, N.; Gimelshein, S.

5d. PROJECT NUMBER

5f. WORK UNIT NUMBER
50260542

7. PERFORMING ORGANIZATION NAME(S) AND ADDRESS(ES)

Air Force Research Laboratory (AFMC)
AFRL/RZSA
1 Ara Drive
Edwards AFB CA 93524-7013

8. PERFORMING ORGANIZATION REPORT NUMBER

9. SPONSORING / MONITORING AGENCY NAME(S) AND ADDRESS(ES)

Air Force Research Laboratory (AFMC)
AFRL/RQR
5 Pollux Drive
Edwards AFB CA 93524-7048

10. SPONSOR/MONITOR'S ACRONYM(S)

11. SPONSOR/MONITOR'S NUMBER(S)
AFRL-RQ-ED-TP-2012-220

12. DISTRIBUTION / AVAILABILITY STATEMENT

Approved for public release; distribution unlimited (PA #12554).

13. SUPPLEMENTARY NOTES
For presentation at the AIAA Thermophysics Conference, New Orleans, LA, 25-28 June 2012.

14. ABSTRACT

A propulsion system based on an array of radiometer vanes has been proposed for wind disturbance correction on near space vehicles. The radiometric force is produced by a vane due to a temperature gradient between a surface heated by insolation and a convectively cooled surface. Previous research has identified several key parameters that might affect the thrust produced by a radiometer array. These parameters include the heat transfer mechanisms on the individual vanes and between nearby vanes in an array, the proximity or spacing of radiometer vanes in an operational array, the effects of the vanes attached to a near space vehicle operating in the boundary layer near the surface of the vehicle, and the effects of attaching the vanes to a substrate on the vehicle itself. A combined numerical and experimental approach was used to investigate these effects. Numerical codes were used to assess the heat transfer mechanisms and the boundary layer flow. Experiments were designed and carried out to measure the force produced by a small array of radiometers. These results were combined to assess the performance of a notional array of radiometer vanes for the purpose of counteracting drag on a near space vehicle operating at an altitude of 60 km. The array performance was assessed based on the maximum force that can be produced as a function of array mass and area.

15. SUBJECT TERMS

16. SECURITY CLASSIFICATION OF:			17. LIMITATION OF ABSTRACT	18. NUMBER OF PAGES	19a. NAME OF RESPONSIBLE PERSON
					Marcus Young
a. REPORT	b. ABSTRACT	c. THIS PAGE			19b. TELEPHONE NUMBER *(include area code)*
Unclassified	**Unclassified**	**Unclassified**	SAR	18	N/A

Thermal Modeling and Performance Measurements of Radiometric Arrays for Near Space Propulsion

Ryan W. Bosworth[1] , Austin L. Ventura[2], and Rebecca N. Webb[3]
University of Colorado Colorado Springs, Colorado Springs, CO 80918

Marcus P. Young[4] and Andrew D. Ketsdever[5]
Air Force Research Lab, Edwards AFB, CA 93524

Natalia E. Gimelshein[6] and Sergey F. Gimelshein[7]
ERC, Inc., Edwards AFB, CA 93524

A propulsion system based on an array of radiometer vanes has been proposed for wind disturbance correction on near space vehicles. The radiometric force is produced by a vane due to a temperature gradient between a surface heated by insolation and a convectively cooled surface. Previous research has identified several key parameters that might affect the thrust produced by a radiometer array. These parameters include the heat transfer mechanisms on the individual vanes and between nearby vanes in an array, the proximity or spacing of radiometer vanes in an operational array, the effects of the vanes attached to a near space vehicle operating in the boundary layer near the surface of the vehicle, and the effects of attaching the vanes to a substrate on the vehicle itself. A combined numerical and experimental approach was used to investigate these effects. Numerical codes were used to assess the heat transfer mechanisms and the boundary layer flow. Experiments were designed and carried out to measure the force produced by a small array of radiometers. These results were combined to assess the performance of a notional array of radiometer vanes for the purpose of counteracting drag on a near space vehicle operating at an altitude of 60 km. The array performance was assessed based on the maximum force that can be produced as a function of array mass and area.

Nomenclature

α	=	absorptivity
C_p	=	specific heat
δ_h	=	separation along vane length
δ_t	=	separation along the axis normal to the vanes
ε	=	emissivity
F	=	force
h	=	thermal convection coefficient
k	=	thermal conductivity

[1] Graduate Research Assistant, Mechanical and Aerospace Engineering, AIAA Student Member.
[2] Undergraduate Research Assistant, Mechanical and Aerospace Engineering, AIAA Student Member.
[3] Assistant Professor, Mechanical and Aerospace Engineering.
[4] Program Manager of Advanced Concepts, Propulsion Directorate, AIAA Member
[5] Senior Research Engineer – Advanced Concepts, Propulsion Directorate, AIAA Associate Fellow
[6] Consultant, AIAA Senior Member
[7] Senior Research Engineer, AIAA Senior Member

Kn	=	Knudsen number
λ	=	mean free path
L	=	radiometer vane edge length
L*	=	characteristic length
P_∞	=	ambient pressure for 60 km altitude
p	=	pressure
ρ	=	density
Q_0	=	insolation energy
$Q_{incident}$	=	incident insolation energy
Θ_{sun}	=	solar inclination angle
T	=	temperature
T_∞	=	ambient temperature for 60 km altitude
ΔT	=	temperature difference between hot and cold sides of a radiometer vane
t	=	vane thickness
t_{bp}	=	baseplate thickness
X	=	relative edge separation
Y	=	relative face separation

I. Introduction

A propulsion system, based on the radiometric force, has been notionally developed in previous research [1] for near space vehicles. The radiometer propulsion system is designed to correct for wind disturbances at altitudes higher than conventional propellers can operate efficiently. The Crooke's radiometer, [2] shown in Figure 1, is a device that produces a force by setting up a temperature gradient across a thin vane submersed in a rarefied gas.

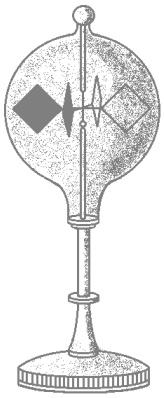

Figure 1. The Crooke's radiometer.

The notional propulsion system uses the radiometric force produced by a multi-vane array operating on solar power and mounted to the surface of the vehicle as shown in Figure 2. [1] The radiometer vane consists of a dark surface to absorb photons and a mirrored surface to reflect photons. The differential absorption sets up a temperature gradient across the two surfaces.

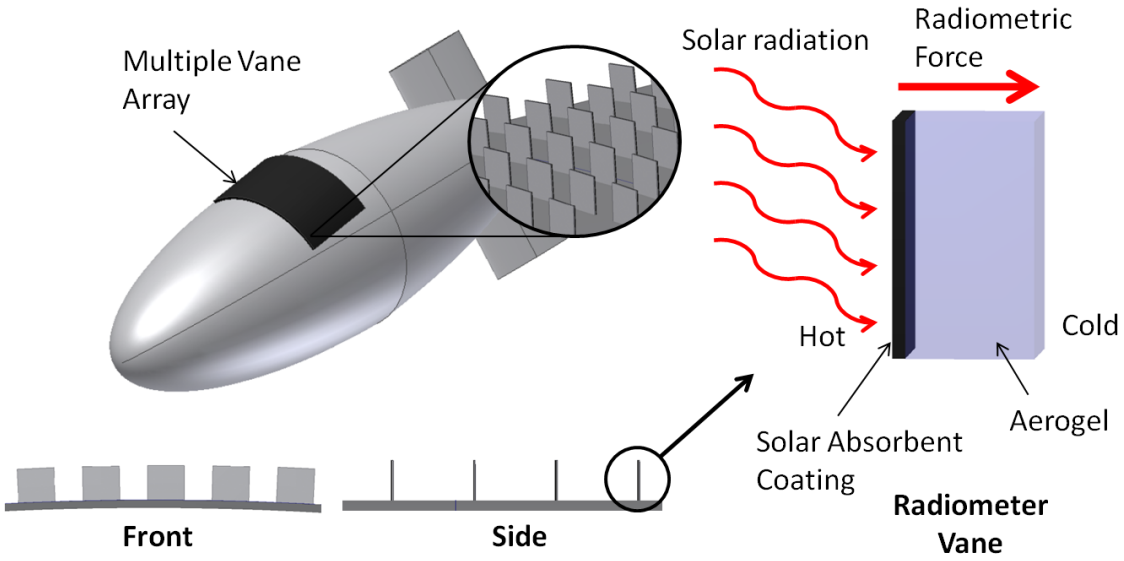

Figure 2. Conceptual propulsion system.

When interacting with a rarefied gas, three forces act on the radiometer vane. [3] The first of these forces is caused by a pressure difference between the gas on the hot side of the vane and that on the cold side. Molecules that collide with the hot side leave with a higher average velocity than those leaving the cold side producing a difference in the momentum flux from each surface. The second force is caused by non-uniform gas heating along the edge of the vane. Molecules near the edge of the vane have a lower probability of colliding with higher energy molecules leaving the vane surface. As a result, the force is greatest near the edge of the vane. Einstein [4] estimated the "edge" force and showed that it occurred within one mean free path of the edge of the vane. The third force is a shear force that acts along the vane thickness. The shear is produced by thermal creep [5] and tends to act in the opposite direction of the other two forces. The contribution of each force varies with the operating pressure and vane geometry. Previous research has shown that the radiometric force is optimized for a Knudsen number of approximately 0.12. The Knudsen number is shown in Equation (1) as the ratio of the gas mean free path to a characteristic dimension in the flow. In this study, square radiometer vanes are being used; therefore, the characteristic dimension used to calculate the Knudsen number is the vane length.

$$Kn = \frac{\lambda}{L^*} \tag{1}$$

Several key factors in determining the performance of the propulsion system were identified by previous research including the heat transfer mechanisms associated with producing a temperature gradient across the vane using insolation, the effects of proximity between vanes (i.e. vane spacing), the effects of vanes operating in a large boundary layer flow near the vehicle surface, and the effects of attaching the vanes to a substrate. The purpose of this research is to investigate the effects these key factors have on performance and update the design of the notional radiometer propulsion system. A combined numerical and experimental approach has been used. Heat transfer mechanisms and the effects of surface properties such as absorptivity, emissivity, and thermal conductivity have been modeled using COMSOL Multiphysics. [6] Experiments have been performed to measure the radiometric force produced by arrays of vanes and for a case of attaching the vane to a substrate. The effects of gas rarefaction on heat transfer, particularly with gas conduction and convection, were modeled in COMSOL using convective heat transfer coefficients found from an Ellipsoidal Statistical kinetic equation (ES-BGK). [7] The same ES-BGK code, in conjunction with a Navier-Stokes solver, was used to assess the effects of boundary layer operation of the vane. Non-zero flow velocity in the boundary layer affects the force produced by a vane. Previous modeling has only considered zero initial flow velocity.

A previous study indicates that the proper operating conditions for a radiometric propulsion system exist between 40 and 80 km in altitude [1]. Accordingly, an operating altitude of 60 km was selected for the propulsion array analysis due to the manufacturing feasibility of the vane size dictated by the ambient pressure. This pressure was taken to be 16.7 Pa with a coinciding ambient temperature of 240 K. These values are obtained from the MSIS-E-90 atmospheric model.

II. Experimental Setup

A. Experimental Technique

The nano-Newton Thrust Stand (nNTS) was selected for force measurements due to its demonstrated ability to accurately measure forces on the order of tens of nano-Newtons [8]. The thrust stand was calibrated by means of the Electro Static Comb Calibration System (ESCCS) [9] before each test. This calibration technique applies known forces to the nNTS and records the deflection of the stand. A direct relationship between force and stand displacement is established. Calibration of the nNTS was completed across the entire range of forces tested before each test. In order to produce a force, the vane(s) needed to interact with a gas. To accomplish this, argon was flowed into the chamber to produce steady state chamber pressures for the experiment as seen in Fig. 3(a). This pressure was varied between 0.1 Pa and 1.5 Pa. The vanes were tested first with no temperature gradient to verify that the thrust stand operation was unaffected by the flow. The result showed a small perturbation of the stand as the flow starts and as the flow is stopped and the gas begins to be pumped out of the chamber. Neither of these events occurred during the steady state operation of the stand used for the data analysis and therefore had no effect on the data. In order to take a single force measurement at a given pressure, the chamber pressure began at 10^{-3} Pa with no argon flow. No flow was introduced to the chamber for the first 30 s of the test, allowing an initial measurement of the stand that was later used for zeroing and drift correcting the data. After 30 s, the argon flow began and a second measurement of stand deflection was taken after the chamber pressure, and consequently the thrust stand reached steady state. Finally, the flow was stopped and the argon was pumped out of the chamber allowing for a final measurement also used in zeroing and drift correction. The chamber pressure as a function of time is shown in Fig. 3(a). Three force measurements were taken for each chamber pressure and chamber pressure was varied from 0.5 to 1.4 Pa. The displacement of the stand was measured using a Linear Variable Differential Transformer (LVDT). This deflection was used to find the thrust force produced at each pressure by using the stand calibration curve generated prior to the experiment with the ESCCS. A typical thrust stand trace used to find the force produced by a given vane geometry is shown in Fig. 3(b)

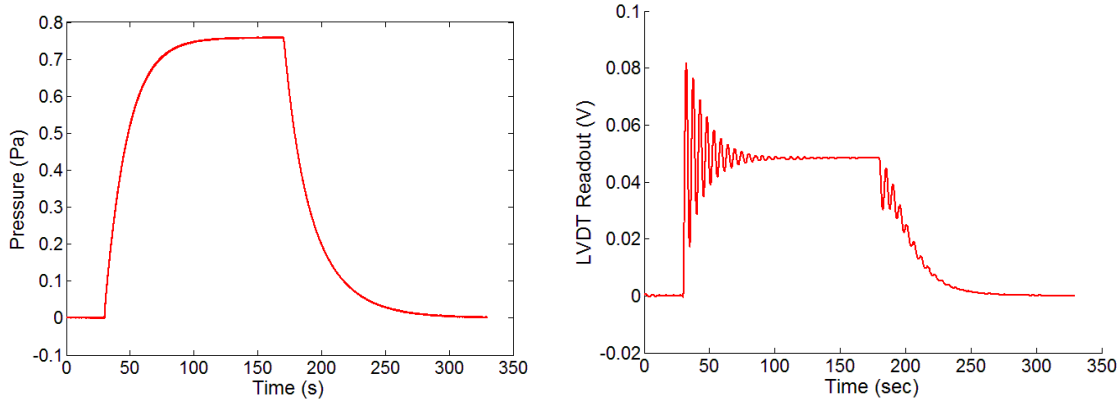

(a) **(b)**

Figure 3. (a) Chamber pressure plot for a test point and (b) a thrust stand trace.

B. Three Vane Array

The force on three vanes with variable spacing was measured. The experiment was performed in a 1 m diameter by 2 m vacuum chamber. A nano-Newton Thrust Stand (nNTS) [8] with an experimentally verified spring constant was used to determine the force generated. A ceramic rod was clamped into a Teflon block at the end of the nNTS to limit heat transfer from the radiometer array to the thrust stand. The test apparatus allowed the separation along the axis normal to the vane face, δ_t to be varied from 15 mm to 80 mm and was attached to the ceramic rod so that the

array was suspended over the middle of the main chamber. The vanes used in the experiment were commercially available Peltier coolers. These consist of two ceramic plates connected by a grid of semiconductors. The vanes measured 40 mm by 40 mm with a thickness of 3.6 mm. Three radiometer vanes were used to create an array along the axis normal to the ceramic plates of the vane as seen in Fig. 4. The separation distance was measured as the distance between the center vane and each of the outside vanes. A temperature difference across each vane was induced by supplying power from a DC voltage source to the semiconductor grids on each of the vanes. The vane array was characterized to find an input power that yielded a temperature difference of approximately 25 K. This temperature difference was experimentally determined by attaching three thermocouples to both faces of all three vanes in the array. Thermal characterization was completed at vacuum with chamber pressures used for testing. The working fluid, argon, was used due its lack of internal modes which facilitates future comparison to numerical models. Results from this setup are used to quantify the effects of multi-vane arrays in order to better characterize a propulsion array.

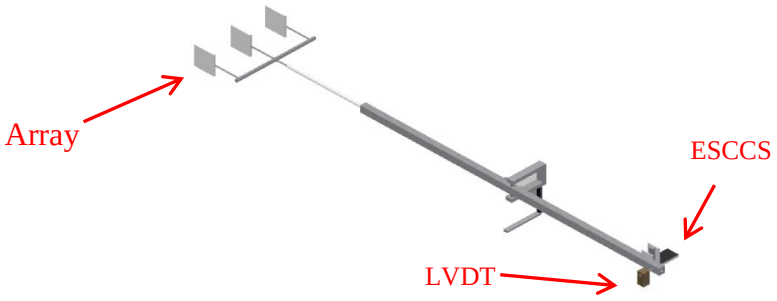

Figure 4. The nNTS with a 3 vane array and the ESCCS and LVDT.

C. Surface Proximity

The effect of surface proximity on force experienced by the vane was measured. Testing for this experiment took place in a larger vacuum chamber than the array testing to limit the effect of chamber wall proximity. The chamber diameter measured to 1.3 m with a length of 2 m. The vane was centered between the door and the rear of the chamber which further reduced chamber contribution to surface proximity effects. A single commercially available thermoelectric cooler was used. A thin, square stainless steel plate, with an edge length of 0.6 m, was suspended above the vane. This plate hung from a linear actuator, allowing in situ changes to the surface proximity. The surface was optically leveled prior to testing. Figure 5 shows the vane attached to the thrust stand in the chamber, with the plate suspended above it. The setup was tested with 2 to 100 mm of separation between the surface and the upper edge of the vane. The temperature of the surface was monitored using 8 thermocouples attached at various points across both sides of the plate. The vane was thermally characterized before testing began. Argon was again used as the working fluid for the experiment. The results of the experiment quantify the change in force as a function of surface proximity in order to predict the effect of attaching the array to a transport vehicle.

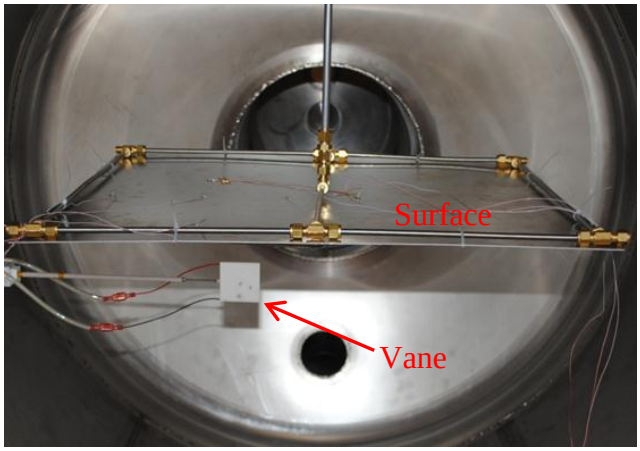

Figure 5. Surface proximity experimental setup.

III. Experimental Results

A. Three Vane Array

For each separation distance, the array was tested across a range of pressures to find the maximum force produced by the array. The test results for a separation distance of 77.71 mm are shown Fig. 6. A similar curve was obtained for each separation distance with each of these data sets being curve fit to find the maximum force. The maximum force produced by any number of vanes consistently occurs at a Knudsen number of 0.12. The force produced by the three vane array increased as the separation between the vanes increased. Results for the maximum force produced by different array spacings are shown in Fig. 7. The separation distance is normalized by vane edge length where the relative face separation is equal to δ_t/L. The dotted line in Fig. 7 represents the force of three radiometer vanes operating completely independently of each other. The data shows that the vanes still have a significant effect on each other even with a vane spacing of two times the edge length. A force increase of 54% was observed for a 600% increase of the vane separation distance. While the increase in force is desirable for the development of a radiometric engine, a higher force per unit surface area of the array will be obtained using a low value for the face separation.

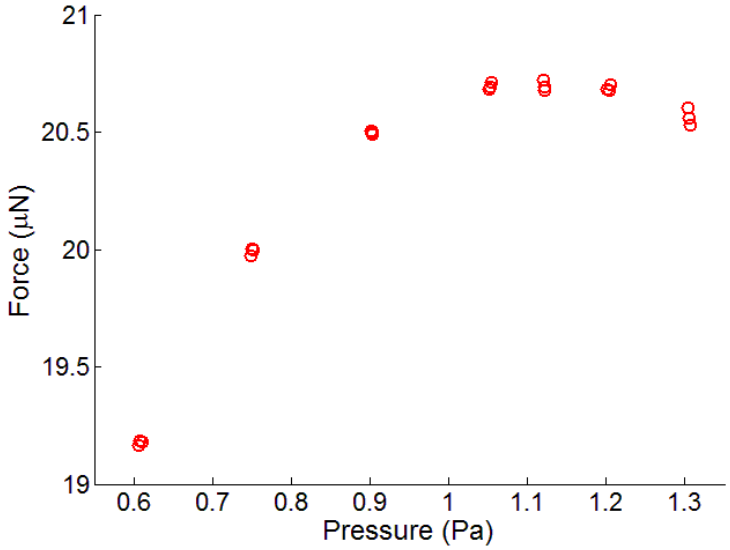

Figure 6. Data curve for a three vane array with a separation of 77.71 mm.

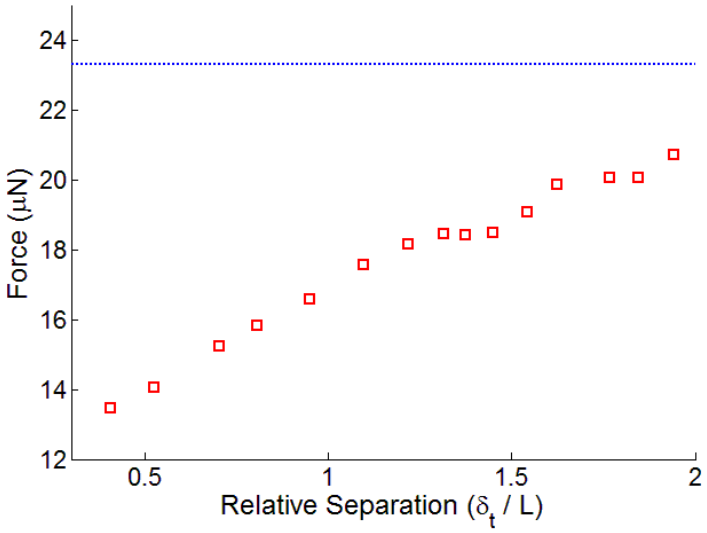

Figure 7. Plot of maximum force produced for each separation.

The results show an approximately linear relationship between forces and face separation. Equation (2) describes the effect of the face separation for relative separation distances less than or equal to 2.5. Above a relative separation of 2.5, the vanes act independently of each other therefore the force produced asymptotes to the value of three times the force of a single vane. C_Y represents the percentage (in decimal form) of the maximum force that an independent vane produces where Y is δ_t/L and is measured in percentage of vane length. Due to the low force increase with face separation the optimization of vane spacing requires the inclusion of thermal modeling results.

$$C_Y = 0.1485(Y) + 0.39 \tag{2}$$

B. Surface Proximity Results

The surface proximity data shows two desirable effects that result from attaching the vanes to the surface of the vehicle. First, an increase in maximum force is produced by placing a single vane near the surface as shown in Fig. 8(a). A separation between the vane edge and the surface of 2 mm yielded an increase of 37% in maximum force produced. Second, the operating pressure corresponding to the maximum force was increased by 30% as seen in Fig. 8(b). The data with a surface proximity of 610 mm represents a vane with no surface in the vacuum chamber, and the chamber wall is used for surface proximity.

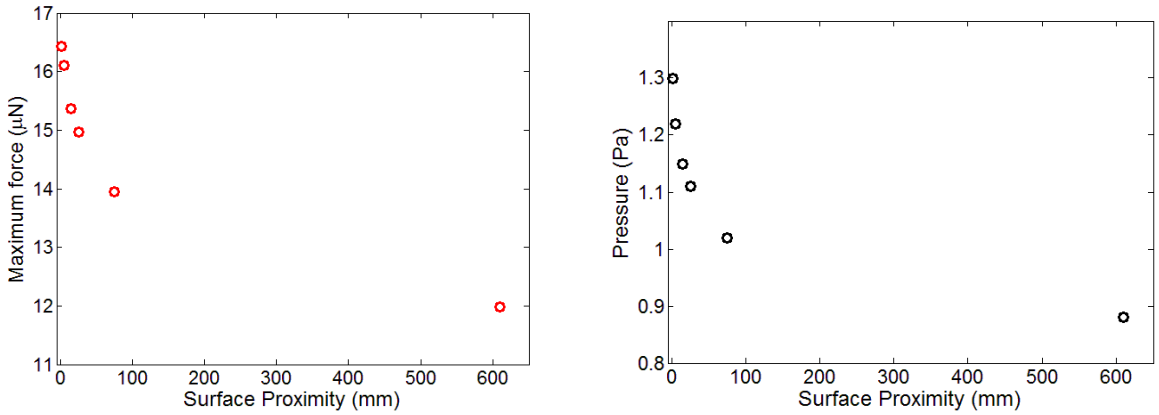

(a) **(b)**

Figure 8. Maximum force (a) and corresponding chamber pressure (b) as a function of surface proximity.

The increase in operating pressure results in a lower mean free path which, from Eq. (1), requires a decrease in the vane edge length in order to maintain a fixed Knudsen number of 0.12. The calculation for the change in L* is shown in Eq. (3). The constants divide out of the equation leaving P_1 as the pressure producing a maximum force with no surface in the chamber, P_2 as the pressure producing a maximum force with the surface at a 2 mm proximity, L_{exp} being the edge length of the tested vane, and L* being the new characteristic length. The percent change in edge length can be obtained by dividing both sides of Eq. (3) by the original vane edge length. This new edge length is calculated to be 67.7% of the original edge length. This decrease is vane size is then taken into account for the calculation of edge length for a vane operating at 60 km. The resulting edge length is 1.57 mm. The force produced by a vane scales approximately with the square root of vane area (L for a square vane) [10], resulting in a greater number of smaller vanes being used in an array that is attached to a vehicle surface. From this, the force results from the testing can be scaled by the factor of L^*/L_{exp} to obtain the force produced by a single vane with an edge length of 1.57 mm.

$$L^* = \frac{P_1 * L_{exp}}{P_2} \tag{3}$$

As the pressure for a vehicle operating at a fixed altitude will remain relatively constant, the data was analyzed to determine the effect of surface proximity on force production at a fixed pressure of 0.9 Pa. Fig. 9 shows the force produced at 0.9 Pa as a function of surface proximity. An increase in force is observed for closer surface proximity to the vane. The force produced by the vane with a 2 mm surface proximity is 32.5% higher than a vane with no surface in the chamber.

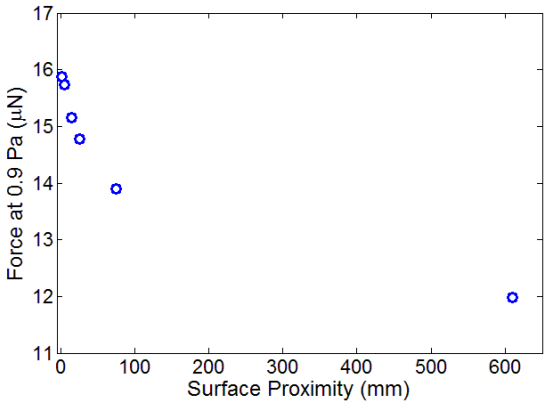

Figure 9. Force produced at 0.9 Pa for a range of proximity values.

IV. Flow Modeling

A. Numerical Set-up

A combined numerical approach was used to model the thermal effects on vane array force production. The convective heat transfer coefficients were determined using a Ellipsoidal Statistical kinetic equation (ES-BGK) and input into COMSOL Multiphysics. The COMSOL model was used to determine the heat transfer mechanisms and the effects of surface properties such as absorptivity, emissivity, and thermal conductivity on the vane array.

The radiometric force over a single vane is expected to reach its maximum for a vane length based Knudsen number of about 0.1. For a radiometer array installed on a near space vehicle that operates at an altitude of about 60 km, this translates to a typical radiometer size on the order of 1.57 mm. This means that numerical analysis of radiometric forces produced by a radiometer array mounted on a large space vehicle has to be two-scale. The first scale is related to the size of the space vehicle, and a typical Knudsen number for such flow is on the order of or less than 10^{-4}, based on the length of the vehicle of at least 10 m. The second scale, with a Knudsen number of about 0.1, is related to the size of a single vane. From the modeling perspective, this splits the whole problem into two parts, where a continuum approach would be used to compute the flow over a near space vehicle, and a kinetic method used to analyze the Knudsen layer flow near a single radiometer vane.

In this work, a Navier-Stokes solver CFD++ [11] is used to compute the flow over a space vehicle, which is modeled here as a 2 m thick and 10 m long ellipsoid. Free stream pressure and temperature of 16.7 Pa and 240 K correspond to an altitude of 60 km. Two free stream velocities, 30 m/s and 100 m/s were considered. The thickness-based Knudsen number is less about 0.0001 for an altitudes of 60 km considered below. CFD++ is an unstructured parallel Reynolds Averaged Navier-Stokes code. It uses a fully implicit, second order in space, second order in time, Harten, Lax, van Leer, Contact discontinuity Riemann approximation algorithm. In the present axisymmetric computations, a single-block grid with a total of about 250,000 nodes is used. The domain size is 50 m in radial direction and 100 m in axial direction. The density-velocity inflow / pressure outflow boundary conditions are used at the boundaries of the computational domain, and an isothermal, 2nd order slip, boundary condition with the wall temperature equal to the free stream value is set at the space vehicle's surface.

The Navier-Stokes calculations are then used to provide the inflow boundary conditions for a kinetic solver SMOKE [12]. SMOKE is based on the solution of the Ellipsoidal Statistical kinetic equation; it is a parallel 2D/axisymmetric finite volume solver for model kinetic equations which uses conservative numerical schemes developed in Ref. [7]. The ES-BGK calculations are performed in a planar 2D geometry, because the size of the computational domain, about 1 cm, is much smaller than the distance from the axis of symmetry, about 1 m. To simulate a large array of tightly spaced radiometers installed on a space vehicle, calculations were conducted with periodic boundary conditions at the left and right boundaries, wall boundary conditions and the bottom boundary, and prescribed inflow boundary conditions from the Navier-Stokes computations at the top boundary. The prescribed boundary conditions were using flow properties from the Navier-Stokes computations. The length of the vane is 2.5 mm, so that Knudsen number based on that length is approximately 0.1. The separation between the vanes was set at 2.5 mm. The temperature difference between the hot and cold sides of the vanes is assumed to be 10 K, with the cold wall temperature equal to the space vehicle's temperature, which is in turn equal to the free stream temperature. The results are for radiometer vanes located at the center of the space vehicle in the axial (flow) direction.

The spatial grid typically consists of about 10,000 cells, and the velocity grid contains (20,18,18) (x,r,θ) points. The space and velocity convergence studies were conducted in earlier studies [10] where radiometric flows with similar Knudsen numbers were examined. To simulate a large array of tightly spaced radiometers installed on a near space vehicle, calculations were conducted in a two-dimensional configuration for a single vane with periodic boundary conditions at the left and right boundaries, wall boundary conditions and the bottom boundary, and prescribed inflow boundary conditions from the Navier-Stokes computations at the top boundary. The prescribed boundary conditions were using flow properties from the Navier-Stokes computations.

B. Numerical Results

The flow velocity field over a near space vehicle is shown in Fig. 10. A close-up of the body is presented to illustrate flow gradients in the boundary layer. The boundary layer is relatively thin, and does not exceed 10% of the body thickness in the central part of the vehicle. Nevertheless, the small Knudsen number results in a significant decrease of velocities near the wall both in the front, where for the 100 m/s case they do not exceed approximately 2 m/s, and especially the rear part of the vehicle, where they drop by over an order of magnitude compared to the front part. Note that caution needs to be used when analyzing these numbers, since the Navier-Stokes solution is known to be questionable in the Knudsen layer. The gas temperature changes less than 1 K across the boundary layer, indicating that the temperature gradient in the surrounding flow should not significant impact the radiometric force. The force production should therefore be governed by temperature gradients across the vane.

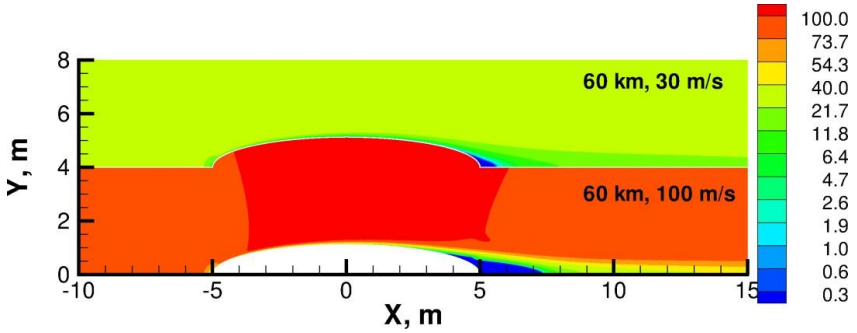

Figure 10. Gas velocity (m/s) in X direction over an elliptic profile for two free stream velocities.

Comparison of velocity profiles in the center of the vehicle, normalized by the corresponding free stream value, is shown in Fig. 11 for two free stream velocities. The small maximum in the flow velocity is observed approximately 10 cm from the body. This location of the maximum flow velocity shifts slightly from the body for the 30 m/s case as compared to the 100 m/s case. The velocity decreases nearly linearly outside the Knudsen layer, which is less than 1 mm thick in the flow conditions under consideration. The inflow boundary conditions for the successive ES-BGK simulations of a radiometer array are set at 1 cm, where the solution is essentially free of any Knudsen layer effects (it is the region of linear decrease of the flow velocity). The boundary conditions for the ES-BGK computations also included gas density and temperature, but the changes in these properties are minor (less than 0.5% from the free stream value for temperature and less than 1% for gas density), and the impact of these is therefore minimal.

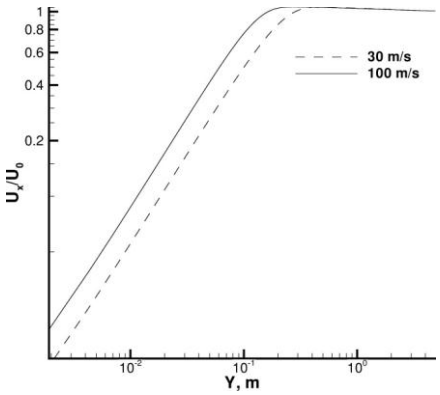

Figure 11. Normalized gas velocity in X direction for two free stream velocities.

Consider now the flow in the vicinity of the vane, obtained though the solution of the ES-BGK equation. Translational temperature fields are shown in Fig. 12. Only the lower half of the computational domain is shown for both flow velocities in order to provide more flow detail. Y=0 for 100 m/s case and Y=0.5 m for the 30 m/s (the latter is shifted 0.5 m upward) correspond to the vehicle's surface. Note that the flow properties at the inflow boundary did not change during the computation, coinciding with the prescribed values. The figure clearly illustrates the interference between the vanes in the considered fairly tight packing, as the temperature gradients are much larger between the vanes than in the vertical direction above the vane. The vehicle surface strongly influences the gas temperature at least up to the central part of the vane. The impact of the flow velocity of gas temperature is relatively small both between the vanes and above them.

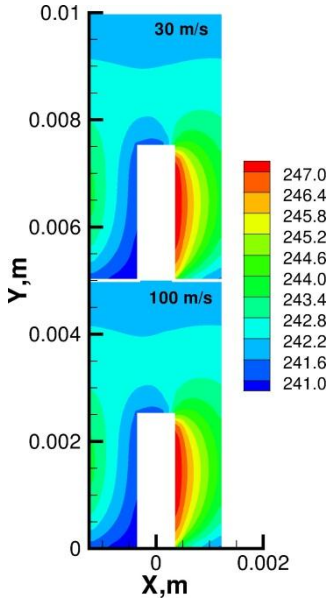

Figure 12. Translational temperature fields (K) near a radiometer vane for two free stream velocities.

The velocity profile along the vertical side of the computational domain (periodic boundary) is shown in Fig. 13. It can be seen that the vane is nearly stopping the flow, so that the velocity is very close to zero for up to 2 mm from the vehicle surface. Close to the wall, the velocity increases more rapidly for the 30 m/s case. However, at the domain boundary the normalized velocity for the 100 m/s case is significantly larger than for the 30 m/s case. It should also be noted that the vanes are located close enough so that the impact of the high temperature at the hot side is felt by the cold side of the radiometer, thus decreasing the radiometric force. However, a smaller separation allows for more closely packed radiometer array, thus increasing its total wind disturbance compensation ability.

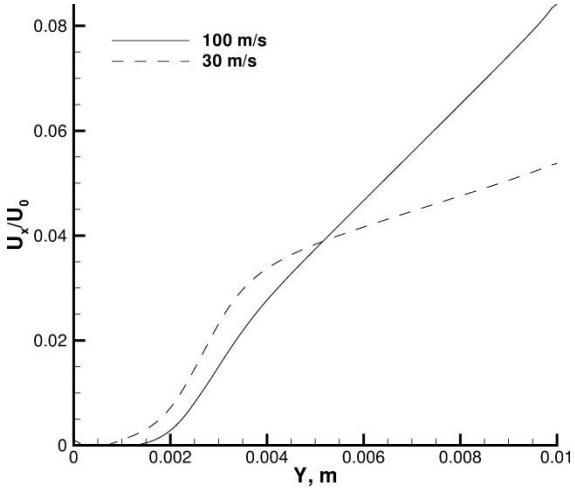

Figure 13. Normalized gas velocity in X direction along the periodic boundary.

The total radiometric force for the different flow conditions is shown in Table 1. In this table, the two free stream velocities under consideration are compared with the no bulk flow case. The values give the force per length for a single radiometer row. A negative force value indicates that the radiometric force acts in the direction opposite to the free stream, and thus proves the ability of a vane to compensate for the wind disturbance. Positive force means that the radiometers move the vehicle in the direction of the drag. The main conclusion that can be drawn from the table is that for head winds up to at least 30 m/s, the radiometer arrays are capable of generating significant wind compensating force. Note also that the difference between the purely radiometric force obtained at zero free stream velocity ($-4.5\text{x}10^{-5}$ N/m) and the total force for a finite free stream velocity is nearly proportional to the velocity at the upper (inflow) boundary of ES-BGK calculation domain, denoted u_{bl} in Table 1.

Table 1.

u, m/s	u_{bl}, m/s	Force, N/m
0	0	$-4.5\text{x}10^{-5}$
30	1.64	$-3.7\text{x}10^{-5}$
100	8.8	$2\text{x}10^{-7}$

V. Heat Transfer Modeling

A. Modeling Set-up

1. Surface Proximity Model

The surface proximity experiment was modeled and the results compared to the experimental findings. The thermoelectric cooler was modeled as a square block with dimensions of 50 x 50 x 5.46 mm. The block was assigned material properties provided by the manufacturer (thermal conductivity = 3.88 W/mK, specific heat = 837 J/kgK, density = 3570 kg/m^3), and with a surface coating with an absorptivity and emissivity of 0.9. The plate was 610 x 610 x 1.59 mm and assigned the thermal properties of 304 stainless steel (thermal conductivity = 14.9 W/mK, specific heat = 477 J/kgK, density = 7900 kg/m^3), and an absorptivity and emissivity of 0.6. The separation distance between the vane and plate was varied from 5 to 200 mm in 5 mm increments. The model was assumed to be within vacuum and the ambient environment which was set at a room temperature value of 296.5 Kelvin.

2. Array Modeling

A station altitude of 60 km, which would be ideal for maximizing radiometric forces, was assumed. Conditions at this altitude were found, according to the MSIS-E-90 model, to be an atmospheric temperature, $T_{\infty,}$ of 240 K and pressure, $P_{\infty,}$ of 16.7 Pa. These external conditions, in conjunction with the experimental results, were used to calculated radiometer vane dimensions for maximum force production. Square vanes with an edge thickness of 1.57 mm and thickness of 0.5 mm were modeled as aerogel (density of 0.01 g/cm^3, thermal conductivity of 0.017 W/mK, and specific heat of 1000 J/kgK).

The energy input was modeled as solar irradiation, represented with a heat flux of Q_0 = 1200 W/m^2. Lambert's cosine law is used to modify the solar influx to the front face of the vanes as the simulated day progresses as indicated in Eqn. (4).

$$Q_{incident} = Q_0 \cos(\theta_{sun}) \tag{4}$$

$Q_{incident}$ is also applied to the top of each vane. A surface-to-surface condition was applied to the front, side, and back faces. Top faces of the vanes were also given a surface-to-ambient radiative condition. A range of emissivities were applied to both the front and back surfaces. A gray body assumption was made. A convection condition was applied to all surfaces. Based off of the numerical work described above, the convective cooling coefficient was set to 21.712 W/m^{2}K. Initially the arrays were not attached to a base plate; a base plate was added to subsequent tests to determine the thermal effects of different attachment surfaces. Base plate materials evaluated include aerogel, Teflon, silicon dioxide, type 304 stainless steel, aluminum, and pure copper (thermal conductivity = 0.017, 0.25, 10.4, 14.9, 237, and 401 W/mK respectively).

Two arrays of vanes were evaluated. In array 1, the vanes were placed in a square grid, and in array 2, each row was 180 degrees out of phase with the row in front of it. Figure 14(a) depicts array 1 and Fig. 14(b) depicts array 2. Initially, the front of each vane is assumed to be a perfect absorber (α=1) while the back, top, and sides are assigned a low absorptivity (α=0.1). Each array was evaluated for a single sun inclination of 30 degrees. Horizontal spacing was set to δ_h = 1.57 mm so in array 2 shadows of leading rows never fall on the row directly behind. The normal axis separation is set as δ_t = 1.57 mm.

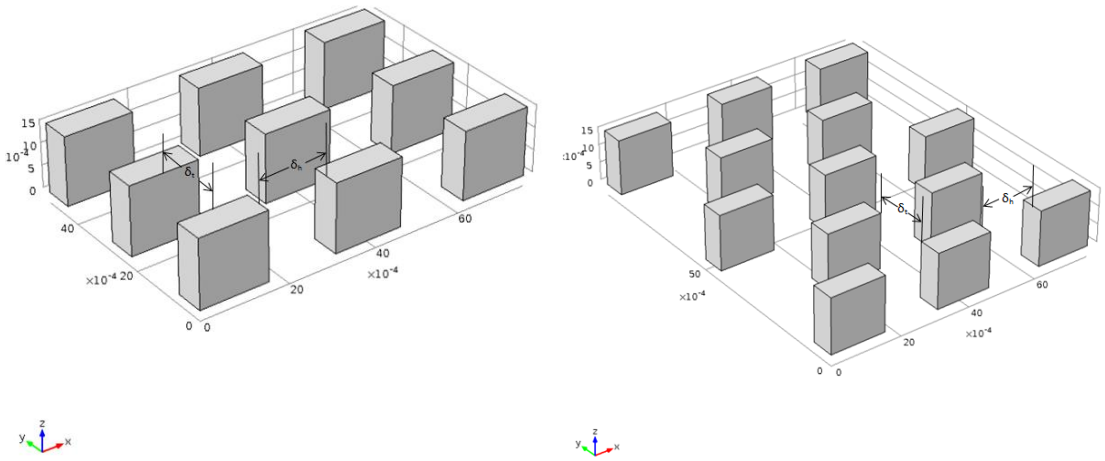

(a) **(b)**

Figure 14. Description of array 1 (a) and array 2 (b) separation distances.

A series of parametric studies were run to determine effect of each parameter on temperature gradient. Studies run are detailed in Table 2. Each parameter was evaluated for a range of insolation values: 1200, 1000, 800, 500, 250, 100, 50, 10, and 1 W/m^2. Lastly, vane thermal conductivity was also varied 0.017, 0.1, 1, 10, and 100 W/mK for the different parameters.

A mesh refinement study was run to verify that the refinement of the mesh had no effect on the results gained. The maximum mesh element size was varied as described in Table 2 with a maximum temperature difference of less than 0.01%. With this determination, all other models were run with an extra fine mesh size which balanced short model times with accuracy in temperature results.

Table 2. Computational modeling test matrix.

Parameter	Minimum Value	Maximum Value	Step Size
Absorptivity of coated front face	0.5	1	0.1
Absorptivity of aerogel	0.1	0.5	0.1
Convection coefficient across vanes (W/m^2*K)	5	40	5
Vane thickness (mm)	0.5	2	0.25
Base plate thickness (mm)	0.15	0.5	0.05
Inline array normal axis separation (mm)	0.57	2.57	0.25
Out of phase array normal axis separation (mm)	0.57	2.57	0.25
Maximum element size for mesh calculation (mm)	0.2	0.9	0.1

B. Modeling Results

1. Surface Proximity

The results of the surface proximity model were compared with the related experiment. The data were found to match within 1 K which is smaller than the resolution of the thermocouples used to measure the experimental values. Figure 15 shows the results for a separation distance of 5 mm. Temperatures of the plate were numerically predicted to range from 297.2 K to 296.6 K while experimental results found an overall average plate temperature of 296.8 K with little variation. The level of agreement verified the use of COMSOL for these and similar evaluations dealing with pressures in transitional and rarefied regimes.

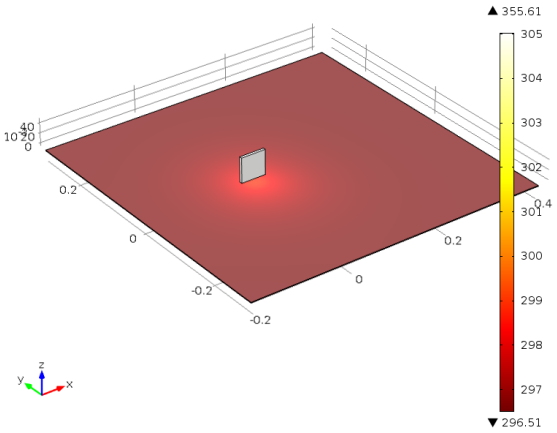

Figure 15. Computed temperature profile for surface proximity model.

2. Array Modeling

The two array configurations were evaluated thermally for several different parameters. The temperature difference across the center vane in each array was determined. For the set sun inclination of 30 degrees, it was determined that when either array 1 and 2 had 25 or more vanes in a 5 x 5 pattern, the center vane could be assumed to be within an infinite array. For this reason, all array configurations evaluated had a minimum of 25 vanes.

The thermal studies that dealt with the thermal conductivity and thickness of the vanes acted as expected. As the thermal conductivity of the vanes increased, the temperature gradient across the length of the vane quickly fell from 13 K to zero due to the fact that the vanes were only 0.5 mm thick. It was also determined that as the vanes' thickness was increased from 0.5 mm to 2 mm, the sustainable temperature gradient also increased from 13 K to 24 K. This is expected but helpful in the understanding that a greater temperature gradient would yield greater force production with the caveat of increased total vane mass.

The temperature profile through the center of the center vane within both array 1 and array 2 was found to be minimally affected by the normal-to-face separation distance, δ_t, until the separations were unrealistically small for the use of insolation as the driving force for the temperature gradient across the vanes. This is indicated in Fig. 16 which shows the temperature gradients through the center of the center vane of array 2 as the separation to vane length ratio, δ_t/L, was changed. Though the overall temperature increases as the vanes come closer together, the total difference remains nearly identical at 13 K. Due to the fact that the gradient was not affected until normal-to-face separations became too small to be feasible, the remaining calculations were evaluated for only array 2 configuration as it allows for closer packed vanes while still realistic for the use of insolation to drive the temperature gradient.

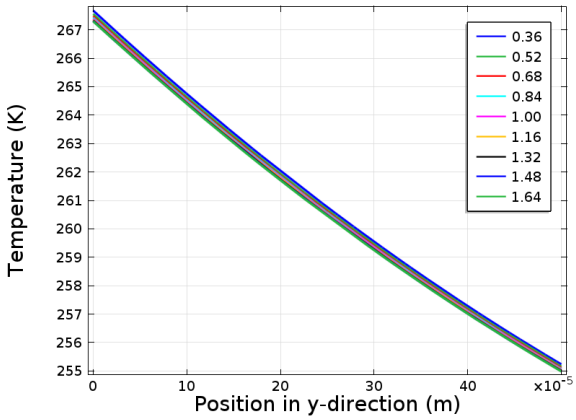

Figure 16. Temperature profile through center of center vane in a 5x5 array 2 configuration for a range of vane separation distances.

The effect surface absorptivity on the sustainable temperature gradient across the vanes was found to be small. The change in absorptivity of the front face had little effect on the temperature difference across the vanes with a 13 K difference with an absorptivity of 1 and a 12.4 K difference with an absorptivity of 0.5. The differing absorptivities on the back, side and top sides of the vane had an even smaller effect on the temperature gradient with a 13 K temperature difference with an absorptivity of 0.1 and a temperature difference of 12.9 K with an absorptivity of 0.5.The result was expected because the front face is the only one receiving direct solar influx. Figure 17(a) describes the evaluated effects of the changing absorptivity of the front vane face and Fig. 17(b) describes the evaluated effects of the changing absorptivity of the back, top, and side faces of the vane.

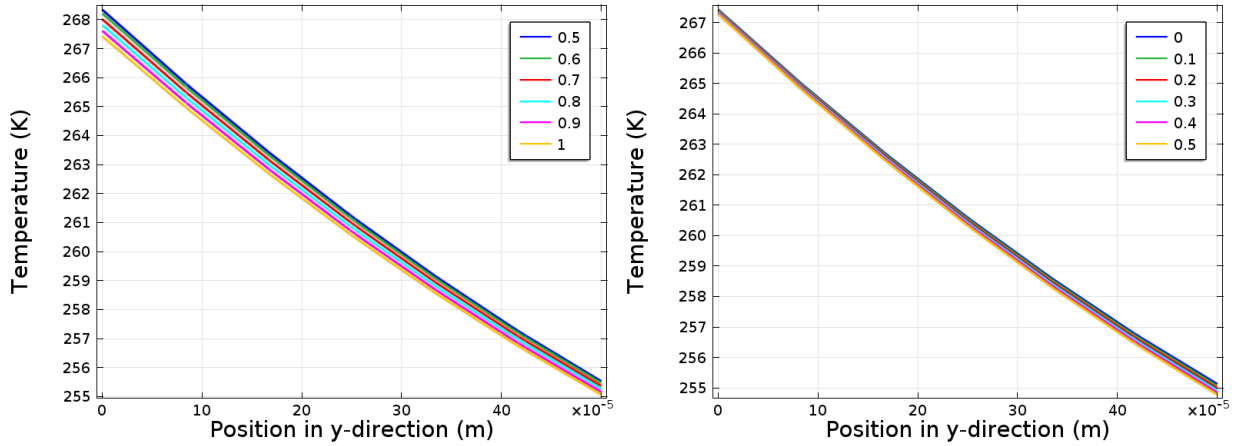

Figure 17. Temperature profile through center of center vane of array 2 for a range of (a) increasing absorptivity on front face and (b) increasing absorptivity of top, side, and back faces.

The total amount of energy introduced into the system greatly affects the vane temperature difference. As solar influx decreases there is less energy available within the vane for conductive, convective, and radiative heat losses which yields a lower temperature gradient as well as lower overall temperatures. Figure 18 shows this effect on the temperature profile through the center vane in an out of phase array. The temperature difference was 13 K with an insolation amount of 1200 W/m^2 and the temperature difference fell to zero as the insolation dropped to zero.

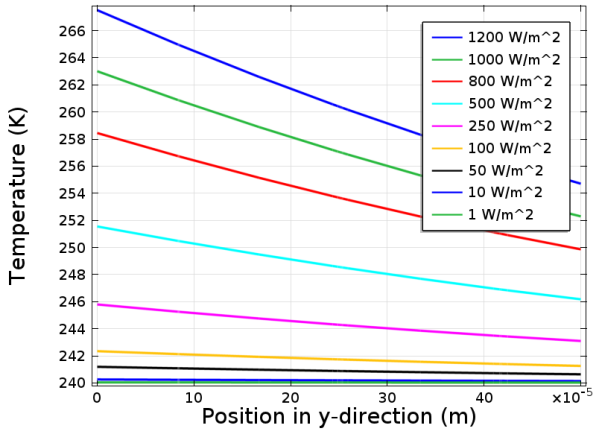

Figure 18. Temperature profile through center of center vane in an array 2 configuration for a range of insolation values.

The sustainable temperature difference was found to be very dependent on the effective convective cooling present on the vane array. This is indicated in Fig. 19 in which the highest temperatures but lowest temperature differences coincide with the smallest convective cooling constants. Conversely, the highest temperature differences matched with the lowest overall temperatures and the highest convective cooling present across the array.

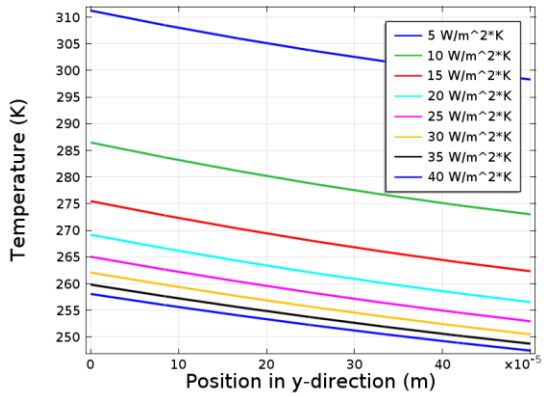

Figure 19. Temperature profile across center vane in a 5x5 array 2 configuration for a range of convection values.

VI. Discussion

A previous experiment [1] has investigated the effect of edge separation on the force production of a three vane array with the vanes aligned edge to edge. The data from this experiment shows that the three vane array will produce 96 percent of the maximum force with a relative separation of 0.7 of the vane edge length. Additionally, the array reaches the maximum force at a relative separation of 1.05. Until the maximum value is reached, the force follows the quadratic trend shown in Eq. (5) and seen in Fig. 20. At a relative separation of 1.05, the vanes begin acting independently of one another.

$$C_x = -0.19X^2 + 0.4X + 0.78 \tag{5}$$

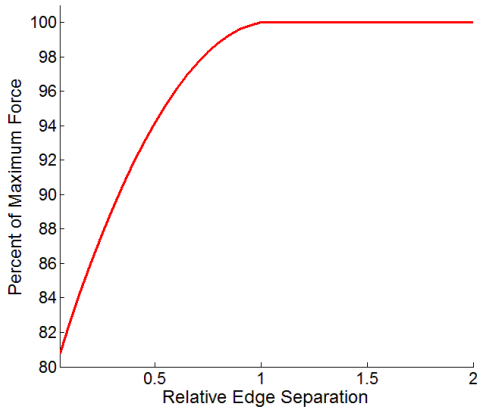

Figure 20. Scaling factor for force as a function of relative edge separation

The combination of experimental and numerical data allows for a better understanding of the contributions of each variable to the overall specifications of the system. As the scaling factors based on edge separation and face separation changed for each array spacing, these were calculated iteratively based on Eq. (2) and Eq. (5). The remaining scaling factors operate independently of the separation variables and were calculated once for the entire range of separation distances. The force production for a vane has been experimentally shown to be proportional to the temperature gradient across the vane. [10] Accordingly, the scaling factor based on temperature is the temperature gradient of the array vanes over the temperature gradient used in the experiment. Since the force produced by a vane varies approximately with the edge length of the vanes, the scaling factor for edge length is the calculated as the edge length of an array vane over the experimental vane edge length. [10] Finally, the experimentally found scaling factor for surface proximity of 132.5% is used to account for the array being attached to the vehicle. Using the above scaling factors, the force produced by a single vane was calculated for relative edge separations between 0 and 2 and relative face separations ranging from 0 to 4. From this information, the number of vanes required to produce 1 N of thrust force was calculated.

Vanes with an edge length of 1.57 mm and a thickness of 0.5 mm were used in the calculation. Determining mass and surface area per unit thrust force allows for easy comparison between designs, and can be easily scaled up to meet specific mission requirements. Since the mass of each vane is unaffected by the separation distances, the mass is then found by multiplying the mass of a single vane times the number of vanes. The mass of the vane is calculated from the specifications used in the thermal modeling. Since results of the thermal modeling show that the absorptivity of the insolated vane face has little effect on the sustainable temperature gradient across the vane, the use of a highly absorbent layer originally described is unnecessary and, therefore, not taken into account in mass calculations. In order to calculate surface area, the required surface area for a single vane is calculated for each vane, as shown in Eq. (6), for each variation of face separation and edge separation.

$$A_{vane} = [t + (X * L)] * [L + (Y * L)] \quad (6)$$

Table 3 shows results for a fixed relative edge separation of 1 while the relative face separation is varied from 0.5 to 2.5. Table 4 shows results for a fixed relative face separation of 2 with the relative edge separation varied from 0.05 to 2.

Table 3. Impact of face separation on array mass and surface area

Relative Face Separation	Array Mass (g)	Array Surface Area (m^2)
0.5	86.48	50.12
1.0	74.69	51.95
1.5	65.72	53.33
2.0	58.68	54.42
2.5	53.00	55.30

Table 4. Fixed face separation and varied edge separation

Relative Edge Separation	Array Mass (g)	Array Surface Area (m^2)
0.05	72.66	12.16
0.5	62.30	32.86
1.0	58.68	54.42
1.5	58.68	77.89
2.0	58.68	101.4

In order to better illustrate the impact of different array geometries, the array surface area and array mass are plotted as a three dimensional surface with the face and edge relative separation distances as the x and y axis respectively. In Fig. 21(a), the z axis represents the surface area of the array and in Fig. 21(b) the z axis represents the mass of the array. Please note the opposite points of view between the two plots.

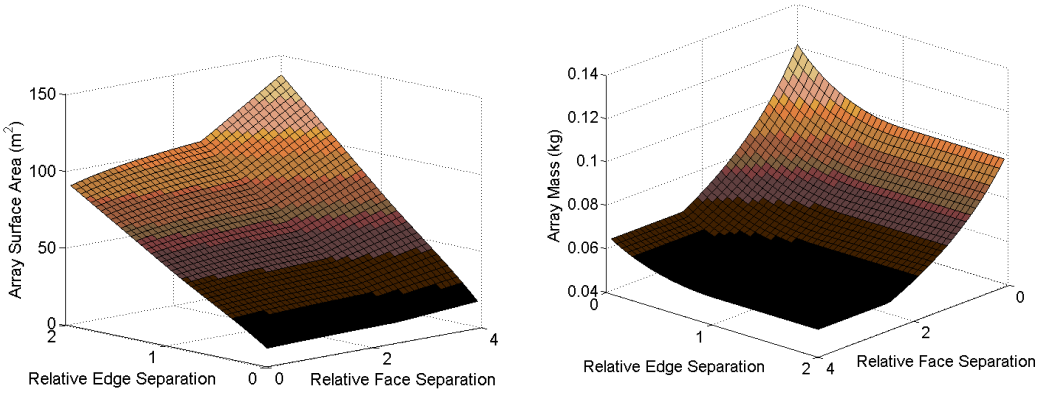

(a) **(b)**

Figure 21. **Array surface area (a) and mass (b) as a function of relative face and edge separations.**

The surface area of the array increases rapidly beyond relative face separations of 2.5. Separations beyond those used in Fig. 21 offer no advantage from a force or thermal interaction standpoint and are therefore not investigated in this work. Additionally, the mass is minimized for a relative edge separation of 1 and a relative face separation of 2.5. The information contained in Fig. 21 will allow for vehicle propulsion system designers to select array geometries that minimize surface area or mass. This data takes into account the all factors considered to have an effect on the force production and provides a thorough analysis of an array operating at 60 km. The scaling factors obtained from the experimental and numerical work of this research can be easily adjusted for different operating conditions. With user specified characteristics of operating altitude, edge separation, face separation, and temperature gradient, the force produced per vane can be easily found by adjusting the scaling factors for each parameter. From this data, the mass and surface area of any radiometric propulsion engine can be determined.

VII: Conclusion

Although results are given only for an array operating at 60 km, the results from this research can be scaled to the desired operating altitude by holding the Knudsen number constant, and solving for the new edge length. As the required force to compensate for wind disturbance will vary by vehicle, the arrays examined here can be scaled to provide the appropriate force. The characterization of a vane operating in close proximity as well as vanes operating in proximity to other vanes provides better understanding of the required vane size and number for a near space propulsion array. Additionally, the thermal interaction modeling provides important information about array spacing and yields an approximation of the temperature gradient for Aerogel vanes operating at 60 km. Future experimental work is planned for testing a scale model of the radiometric array as well as experimentally finding the temperature gradients across Aerogel vanes when exposed to a solar simulator.

Acknowledgments

The authors wish to acknowledge the support of the Air Force Research Laboratory's Propulsion Directorate Advanced Concepts Group.

References

[1] Cornella B., Ketsdever A., Gimelshein S., and Gimelshein N., "Analysis of Multi-Vane Radiometer Arrays in High-Altitude Propulsion" *AIAA paper 2010-4516*, 10th Joint Thermophysics and Heat Transfer Conference, Chicago, IL, USA ,2010.

[2] Crookes W., "On attraction and repulsion resulting from radiation," Phil. Trans. R. Soc. of London, 164:501-527.

[3] Kennard, E. h., Kinetic Theory of Gasses, Mcgraw-Hill, New York 1938.

[4] Einstein, A., "Zur theorie der radiometrerkrafte," Z. Physik, 27:1, 1924.

[5] Sone, Y., Molecular Gas Dynamics: theory, techniques, and applications," Birkhauser, Boston, 2007.

[6] COMSOL Multiphysics, Software Package, Ver. 4.2a, COMSOL Group, Stockholm, Sweden,2011

[7] L. Mieussens, "Discrete-Velocity Models and Numerical Schemes for the Boltzmann-BGK Equation in Plane and Axisymmetric Geometries," *Journal of Computational Physics,* 2000, Vol.162, pp.429-466.

[8] Jamison A. J., "Accurate Measurement of Nano-Newton Thrust for Micropropulsion System Characterization," 27th International Electric Propulsion Conference, Pasadena, California, USA, IEPC-01-236.

[9] Selden, N., Ketsdever, A., "Comparison of Force Balance Calibration Techniques for the Nano-Newton Range,"

Review of Scientific Instruments, Vol. 74, No. 12, December 2003.

[10] N. Selden, C. Ngalande, N. Gimelshein, S. Gimelshein and A. Ketsdever, "Origins of radiometric forces on a circular vane with a temperature gradient," *Journal of Fluid Mechanics*, 2009, Vol. 634, pp 419-431.

[11] S. Chakravarthy and O. Peroomian, "Some internal flow applications of a unified-grid CFD methodology, AIAA Paper 96-2926.

[12] D.C. Wadsworth, N.E. Gimelshein, S. F. Gimelshein, I.J.Wysong, "Assessment of Translational Anisotropy in Rarefied Flows Using Kinetic Approaches," *Proc. XXVI Int. Symp. on Rarefied Gas Dynamics*, Kyoto, Japan, July 2008.